

Longitudinal Structure Function at the Limit $x = Q^2/s$

G. R. Boroun*

Department of physics, Razi University, Kermanshah 67149, Iran

(Dated: July 23, 2025)

The longitudinal structure function for nucleons and nuclei is considered at fixed \sqrt{s} and Q^2 to the minimum value of x given by Q^2/s . This is done using the expansion method and color dipole model in the next-to-leading order approximation. The extracted longitudinal structure functions were consistent with HERA hepdata [<https://www.hepdata.net/record/ins1377206>] and the determination of F_L at $x = Q^2/s$ [Frank E.Taylor, Phys. Rev. D **111**, 052001 (2025)] at moderate and large Q^2 values. The results, consistent with the dipole picture at low Q^2 values, show that the longitudinal structure function is small as expected due to the transverse polarization of the exchanged photon and the strong suppression of the dominant gluon component. Nonlinear corrections to the nuclear longitudinal structure function at low values of x and Q^2 are also considered. These results may enhance the deep inelastic scattering neutral current data in future colliders at low x and low Q^2 .

I. INTRODUCTION

The longitudinal structure function, $F_L(x, Q^2)$, is a fundamental observable in deep inelastic scattering (DIS) experiments, as in the first approximation of the parton model, it is equal identically zero [1] since in the naive quark-parton model (QPM) the massless spin- $\frac{1}{2}$ partons cannot absorb the longitudinally polarized photon. The knowledge of the longitudinal structure function at small values of the Bjorken variable x is important for understanding the inside structure of hadrons (like protons) using high-energy lepton collisions in future such as the Large Hadron electron Collider (LHeC) [2] at CERN and the Electron-Ion Collider (EIC) [3] at Brookhaven National Laboratory (BNL) in e-A scattering.

The longitudinal structure function helps test quantum chromodynamics (QCD) predictions beyond leading order (LO) and provides constraints on the gluon density crucial for LHC predictions. It is sensitive to higher-twist effects and non-linear QCD dynamics at very small x , and it is important for precision Standard Model tests and searches for new physics. In the QCD improved parton model, it provides important information about the quarks and gluon distribution functions of the target. The measured longitudinal structure function $F_L(x, Q^2)$ is related to the cross section σ_L for absorption of longitudinally polarized virtual photon by

$$F_L(x, Q^2) = \frac{Q^2}{4\pi^2\alpha_{em}}(1-x)\sigma_L(x, Q^2), \quad (1)$$

and is related to the transverse structure functions by

$$F_L(x, Q^2) = F_2(x, Q^2) - 2xF_1(x, Q^2). \quad (2)$$

The longitudinal structure function has been measured at HERA (electron-proton collider) and in fixed-target experiments. It is extracted from cross-section measurements at different beam energies and determined in the high inelasticity (y) at the HERA collider. HERA collected the electron-proton (ep) data at various x and Q^2 values for different \sqrt{s} values, where s is the total energy squared of the electron-proton scattering. These analyses have been conducted by the H1 [4] and ZEUS [5] collaborations. H1 covered a kinematic range from $Q^2 = 1.5 \text{ GeV}^2$ and $x = 0.279 \times 10^{-4}$ up to $Q^2 = 800 \text{ GeV}^2$ and $x = 0.0322$. ZEUS data has been taken in much smaller region from $Q^2 = 9 \text{ GeV}^2$ up to $Q^2 = 110 \text{ GeV}^2$. These kinematics will be extended down to $x \simeq 10^{-7}$ at the Future Circular Collider electron-hadron (FCC-eh) [6] with a center-of-mass energy of $\sqrt{s} \simeq 3.5 \text{ TeV}$ at a similar luminosity as the LHeC with $\sqrt{s} \simeq 1.3 \text{ TeV}$. This is about four times the center-of-mass energy range of ep collisions at HERA [7, 8]. On the other hand, the center-of-mass energy at the EIC will be approximately $\sqrt{s} \simeq 140 \text{ GeV}$ which is lower than the flagship HERA data. These new colliders will enable the investigation of lepton-hadron processes in ultra-high

*Electronic address: boroun@razi.ac.ir

energy (UHE) neutrino astroparticle physics.

One of the main topics in hadron physics in the new accelerators at small x limit is the Color Glass Condensate (CGC) effective field theory [9, 10] in the dipole frame [11, 58]. Saturation models [13, 14] and geometrical scaling [15, 16] can successfully describe HERA data in the small x and low Q^2 region. Future electron-nucleus colliders are the best candidates for discriminating between these models and the CGC physics. The CGC forms the initial state, which is important in itself as a new state of matter that depends on the unintegrated gluon distribution (UGD). The next-to-leading-order (NLO) corrections to the cross section for the inclusive production of a pair of hard jets using the color dipole picture for photon-nucleus interactions at small x are discussed in Ref.[17]. The importance of including a finite size for the target on observables sensitive to small- x evolution within the CGC is discussed in Ref.[18]. The prospects for extracting the longitudinal proton structure function at the EIC, which is a highly competitive direct probe of the proton gluon density, are explored in Ref.[19].

The reduced cross section for inclusive e-p NC DIS (neutral current deep inelastic scattering) depends on the DIS structure functions, F_2 and F_L , as they include terms of photon, photon-Z boson interference, and direct Z boson interaction terms. In the kinematic range discussed above, the factors dependent on Z-boson exchange are small. Therefore the reduced cross section is as follows:

$$\sigma_r(x, Q^2, s) = F_2(x, Q^2) - \frac{y^2}{Y_+} F_L(x, Q^2), \quad (3)$$

where $Y_+ = 1 + (1 - y)^2$ and $y = Q^2/(xs)$. Recently, Frank E.Taylor [20] has discussed the longitudinal structure function based on an extrapolation of the reduced neutral current cross section with HERA data at a fixed \sqrt{s} and Q^2 at $x_{\min} = Q^2/s$, where indicate that the longitudinal polarization of the virtual photon at $y = 1$ is zero¹. Therefore the measurement of the reduced cross section in this limit is a determination of the transversely polarized photon-parton scattering. The reduced cross section, in this limit, is given by

$$\lim_{y \rightarrow 1} [\sigma_r(x, Q^2, s)] = F_2(Q^2/s, Q^2) - F_L(Q^2/s, Q^2) = 2 \frac{Q^2}{s} F_1(Q^2/s, Q^2). \quad (4)$$

This limit shows several properties consistent with the dipole picture such as the effect of parton saturation [22] at very low Q^2 . A connection between the longitudinal DIS structure function and the differential cross-section for single-inclusive jet production with transverse momentum dependent (TMD) is considered in Ref.[23] at small Bjorken x . They show that the single-inclusive jet cross-section in longitudinally polarised DIS at leading power (LP) in P_\perp/Q and small x depends on gathering the quark and gluon jet contributions. Some analytical solutions of the longitudinal DIS structure function have been reported in recent years [24–38].

In DIS on nucleon targets, it is well known that an additional constraint at x_{\min} on the gluon distribution determines the transversely polarized photon-parton scattering, which comes from measuring the longitudinal structure function F_L . On the other hand, due to the poor determination of the nuclear gluon distribution, measurements of F_L on nuclear targets would be of great importance in EIC colliders. This would help constrain the gluon distribution and study the nuclear dynamics at x_{\min} . In fact, studies within perturbative QCD and model calculations show that the corresponding nuclear effects closely follow those on the gluon distribution at x_{\min} [51].

In this paper, an analytical distribution based on the expansion method at the next-to-leading order (NLO) approximation is extended to explore the longitudinal structure function at the kinematic point $y = 1$ (corresponding to $x_{\min} = Q^2/s$) in nucleons and nuclei. The longitudinal structure function approaches zero at this point, and this behavior could be beneficial for nucleon and nuclei parametrization groups.

II. METHOD

The longitudinal structure function can be related to the parton distribution functions at small x by ignoring the nonsinglet distribution function. This relationship can be written as [39, 40]

$$F_L(x, Q^2) = \langle e^2 \rangle [C_{L,q}(x, a_s) \otimes x \Sigma(x, Q^2) + C_{L,g}(x, a_s) \otimes x g(x, Q^2)], \quad (5)$$

¹ The virtual photon can be polarized into transverse and longitudinal polarizations at low values of x [21]. The longitudinal polarization of the virtual photon is given by $\epsilon = \frac{2(1-y)}{Y_+}$.

where $a_s = \alpha_s/4\pi$ and $\langle e^2 \rangle = \sum_{i=1}^{n_f} e_i^2/n_f$ with the charge e_i for the active quark flavours (n_f). Here $F_{2s}(x, Q^2) = x\Sigma(x, Q^2) = x \sum_{i=u,d,s,c,\dots} (q_i(x, Q^2) + \bar{q}_i(x, Q^2))$ and $G(x, Q^2) = xg(x, Q^2)$ are the singlet and gluon distribution functions in the fractional hadron momentum. The perturbative expansion of the coefficient functions is as follows

$$C_{L,i}(x, a_s) = \sum_{n=1} \left(\frac{\alpha_s}{4\pi}\right)^n c_{L,i}^{(n)}(x). \quad (6)$$

where the coefficient functions in the LO approximation read [41]

$$C_{L,q}^{(1)}(x) = 4C_F x, \quad C_{L,g}^{(1)}(x) = 8n_f x(1-x), \quad (7)$$

where $C_F = 4/3$ in QCD. The coefficient functions in the NLO approximation at small fraction momentum read

$$C_{L,q}^{(2)}(x)_{x \ll 1} \simeq -2.370 \frac{n_f}{x}, \quad C_{L,g}^{(2)}(x)_{x \ll 1} \simeq -5.333 \frac{n_f}{x}. \quad (8)$$

By applying the convolution integral, the longitudinal structure function can be rewritten as

$$F_L(x, Q^2) = \sum_{n=1} \left(\frac{\alpha_s}{4\pi}\right)^n \int_0^{1-x \approx 1} dz \left[c_{L,q}^{(n)}(1-z) F_2\left(\frac{x}{1-z}, Q^2\right) + \langle e^2 \rangle c_{L,g}^{(n)}(1-z) G\left(\frac{x}{1-z}, Q^2\right) \right]. \quad (9)$$

With expanding the distribution functions around the point $z = a$ [42–47] ($0 \leq z \lesssim 1$) as the following series is convergent for $|z - a| < 1$, we find:

$$F_L(x, Q^2) = \frac{2\alpha_s}{3\pi} F_2\left(\frac{x}{1-a}\left(\frac{4}{3} - a\right), Q^2\right) + \frac{10\alpha_s}{27\pi} G\left(\frac{x}{1-a}\left(\frac{3}{2} - a\right), Q^2\right) - 9.480 \left(\frac{\alpha_s}{4\pi}\right)^2 \frac{\frac{3}{2} - 2a}{(1-a)^2} F_2\left(\frac{\frac{3}{2} - 2a}{(1-a)^2} x, Q^2\right) - 5.926 \left(\frac{\alpha_s}{4\pi}\right)^2 \frac{\frac{3}{2} - 2a}{(1-a)^2} G\left(\frac{\frac{3}{2} - 2a}{(1-a)^2} x, Q^2\right). \quad (10)$$

At the point where $z = 0.5$ is expanding (for further expanding points refer to Appendix A), Eq. (10) can be rewritten in the following simplest form:

$$F_L(x, Q^2) = \frac{2\alpha_s}{3\pi} F_2\left(\frac{5}{3}x, Q^2\right) + \frac{10\alpha_s}{27\pi} G(2x, Q^2) - \frac{18.960\alpha_s^2}{16\pi^2} F_2(2x, Q^2) - \frac{11.852\alpha_s^2}{16\pi^2} G(2x, Q^2) = \frac{10\alpha_s}{27\pi} G(2x, Q^2) \left[1 + \frac{9}{5} \frac{F_2(\frac{5}{3}x, Q^2)}{G(2x, Q^2)} \right] - \frac{11.852\alpha_s^2}{16\pi^2} G(2x, Q^2) \left[1 + \frac{18.960}{11.852} \frac{F_2(2x, Q^2)}{G(2x, Q^2)} \right]. \quad (11)$$

At small x , the right-hand side is dominated by the gluon contribution. In fact, the ratio F_2/G is less than 0.1 in a wide range of x ($x < 0.1$) and Q^2 . Therefore, Eq. (11) can show that

$$F_L(Q^2/s, Q^2) \simeq \left[\frac{10\alpha_s}{27\pi} - \frac{11.852\alpha_s^2}{16\pi^2} \right] G(2Q^2/s, Q^2), \quad (12)$$

where the gluon distribution is obtained using a dipole model fit (Appendix B) to low- x data on F_2 in the following form [48]

$$G(x, Q^2) = \frac{3\sigma_0}{4\pi^2\alpha_s} \left[-Q^2 e^{-Q^2(x/x_0)^\lambda} + (x_0/x)^\lambda \left(1 - e^{-Q^2(x/x_0)^\lambda} \right) \right]. \quad (13)$$

Therefore we find the longitudinal structure function at the limit $x = Q^2/s$

$$F_L(Q^2/s, Q^2) = \left[\frac{10\alpha_s}{27\pi} - \frac{11.852\alpha_s^2}{16\pi^2} \right] \frac{3\sigma_0}{4\pi^2\alpha_s} \left[-Q^2 e^{-Q^2(\frac{2}{x_0}(Q^2/s + 4m_c^2/s))^\lambda} + (x_0/(2(Q^2/s + 4m_c^2/s)))^\lambda \left(1 - e^{-Q^2(\frac{2}{x_0}(Q^2/s + 4m_c^2/s))^\lambda} \right) \right]. \quad (14)$$

Since the photon wave function depends on the mass of the quarks in the $c\bar{c}$ dipole in the dipole cross section, we have modified the Bjorken variable x to the rescaling variable χ , where $\chi = \frac{Q^2}{s} + \frac{4m_c^2}{s}$ as reduced to the the Bjorken variable x at high Q^2 values. This modification is consistent with the general mass-variable flavor number scheme

(GM-VFNS) in parameterization models.

Recently, the authors in Ref.[49] modified the dipole cross section with simulated nonlinear QCD evolution by introducing a rescaling in the saturation scale as $Q_s^2(x) \rightarrow k \cdot Q_s^2(x)$. The parameter k can be understood as a factor that controls the strength of the triple Pomeron vertex and, therefore, the significance of nonlinear dynamics. A value of $k = 0$ corresponds to the linear behavior of the dipole cross section, while $k = 1$ results in the dipole cross sections fitted to HERA data. Finally, for $k > 1$, there is an additional enhancement of nonlinear effects. The nuclear enhancement of the saturation scale, which corresponds to an increase in the density of gluons, is defined on a large nucleus rather than a single proton. In this case, $Q_s^2(x) \rightarrow Q_{s,A}^2(x)$, where $Q_{s,A}^2(x)$ represents the saturation scale for the nuclear target.

We now use the DIS F_L on electron-proton collisions to make predictions for electron-ion collisions with the replacements [63] $S \rightarrow S_A = A^{2/3}S$, where S is the area of the target and the transverse size of the dipole cross section scaling is approximately proportional to $\sim A^{2/3}$, and $Q_s^2(x) \rightarrow Q_{s,A}^2(x) = A^{1/3}Q_s^2(x)$ where $Q_s^2(x) = Q_0^2(x/x_0)^{-\lambda}$ with $Q_0^2 = 1 \text{ GeV}^2$. The nuclear longitudinal structure function at the limit $x = Q^2/s$ is

$$F_L^A(Q^2/s, Q^2) = \left[\frac{10\alpha_s}{27\pi} - \frac{11.852\alpha_s^2}{16\pi^2} \right] \frac{3\sigma_0 A^{2/3}}{4\pi^2 \alpha_s} \left[-Q^2 e^{-\frac{Q^2}{A^{1/3}} \left(\frac{x_0}{2} (Q^2/s + 4m_c^2/s) \right)^\lambda} + A^{1/3} \left(x_0 / (2(Q^2/s + 4m_c^2/s)) \right)^\lambda \left(1 - e^{-\frac{Q^2}{A^{1/3}} \left(\frac{x_0}{2} (Q^2/s + 4m_c^2/s) \right)^\lambda} \right) \right]. \quad (15)$$

The nuclear DIS structure functions in recent years by several methods have been proposed in Refs.[51–58].

III. RESULTS AND DISCUSSION

The standard representation for QCD couplings in the LO and NLO (within the $\overline{\text{MS}}$ -scheme) approximations reads

$$\begin{aligned} \alpha_s(t) &= \frac{4\pi}{\beta_0 t} & (\text{LO}), \\ \alpha_s(t) &= \frac{4\pi}{\beta_0 t} \left[1 - \frac{\beta_1 \ln \ln(t)}{\beta_0^2 t} \right] & (\text{NLO}), \end{aligned}$$

with β_0 and β_1 as the first two coefficients of the QCD β -function,

$$\beta_0 = \frac{1}{3}(11C_A - n_f), \quad \beta_1 = \frac{1}{3}(34C_A^2 - 2n_f(5C_A + 3C_F)),$$

where $C_F = \frac{N_c^2 - 1}{2N_c}$ and $C_A = N_c$ are the Casimir operators in the fundamental and adjoint representations of the $\text{SU}(N_c)$ color group, and $t = \ln \frac{Q^2}{\Lambda^2}$ where the QCD parameter Λ for active flavors has been determined [26] based on $\alpha_s(M_z^2) = 0.1166$,

$$\begin{aligned} \text{LO} : \Lambda(n_f = 3) &= 0.1368 \text{ GeV}, \quad \Lambda(n_f = 4) = 0.1368 \text{ GeV}, \quad \Lambda(n_f = 5) = 0.8080 \text{ GeV}, \\ \text{NLO} : \Lambda(n_f = 3) &= 0.3472 \text{ GeV}, \quad \Lambda(n_f = 4) = 0.2840 \text{ GeV}, \quad \Lambda(n_f = 5) = 0.1957 \text{ GeV}. \end{aligned} \quad (16)$$

In Figs.1 and 2, we compare the longitudinal structure function at the limit of $x = Q^2/s$ for $\sqrt{s} = 318$ and 300 GeV respectively. This comparison is made with the e^+p HERA data, as shown in Tables 1 and 2 of Ref.[59]. These tables combine the reduced cross section datasets from H1 and ZEUS, along with their respective kinematic regions. The extracted longitudinal structure functions are shown as a function of Q^2 and x_{min} in Tables VIII and IX of Ref.[20], accompanied by the uncertainties of the data points. The results at the LO and NLO approximations are obtained from the gluon distribution behavior using a dipole picture [48]. We observe that this distribution accurately represents the longitudinal structure function at both low and high Q^2 values, consistent with the HERA data. The longitudinal structure functions obtained from the dipole picture show that F_L is small at low x and low Q^2 because the polarization of the exchanged photon is transverse at this kinematic point. The results in Figs.1 and 2 correspond to the four active flavors (i.e., $n_f = 4$) while considering the rescaling variable, i.e., Eq. (20).

The effects of the rescaling variable in the longitudinal structure function are shown in Fig.3. We observe that the behavior of $F_L(Q^2/s, Q^2)$ is affected by the large quark mass $m_c \approx 1.4 \text{ GeV}$, whether or not the rescaling variable is

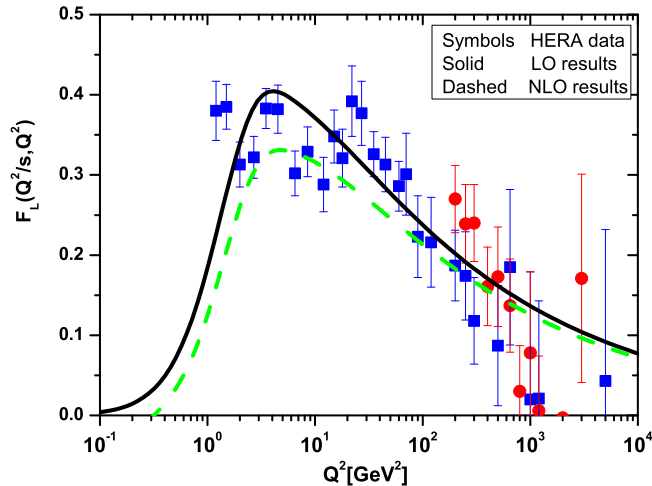


FIG. 1: The DIS longitudinal structure functions at LO (black solid curve) and NLO (green dashed curve) approximations are shown as a function of Q^2 for $\sqrt{s} = 318$ GeV. These results consider the charm effect in the rescaling of the Bjorken variable x . The coefficients are based on the results from Fit 1 in Table I. The HERA combined H1 and ZEUS reduced cross section datasets (squares-blue and circles-red) and their uncertainties are shown.

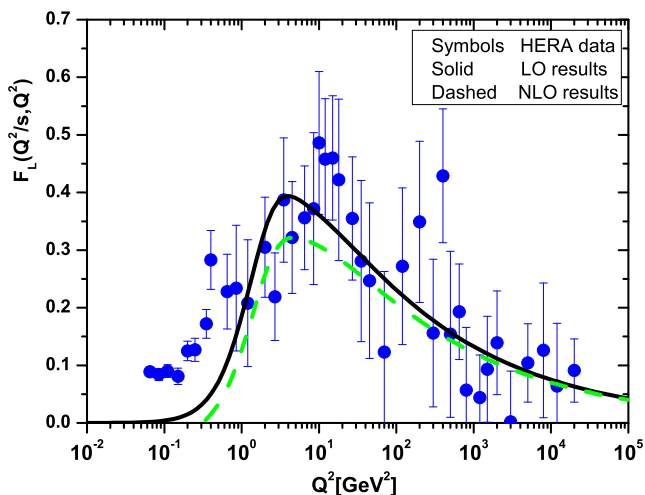


FIG. 2: The same as Fig.1 at $\sqrt{s} = 300$ GeV.

used. When comparing with HERA data, the comparison without rescaling shows lower quality at moderate Q^2 . However, the comparison is significantly improved with scaling.

This rescaling strongly depends on the mass of the quarks in the $q\bar{q}$ dipole. In Fig.4, we show the mass effects of the rescaling variable in $F_L(Q^2/s, Q^2)$. We observe that adding charm into the analysis improves the results at low and moderate Q^2 values compared to the contributions of light and bottom quarks. Nevertheless, the parameters of the bottom quark contribution can be taken into account for further analysis in order to have a full understanding of heavy quarks [62].

In Fig.5, we show the behavior of the DIS longitudinal structure function divided by A at the NLO approximation

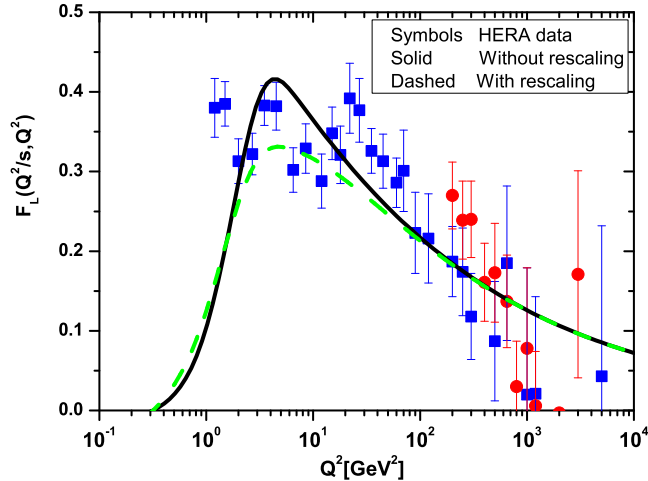


FIG. 3: The DIS longitudinal structure functions without rescaling (black solid curve) and with rescaling (green dashed curve) approximations at the NLO approximation are shown as a function of Q^2 for $\sqrt{s} = 318$ GeV. The coefficients are based on the results from Fit 1 in Table I. The HERA combined H1 and ZEUS reduced cross section datasets (squares-blue and circles-red) and their uncertainties are shown.

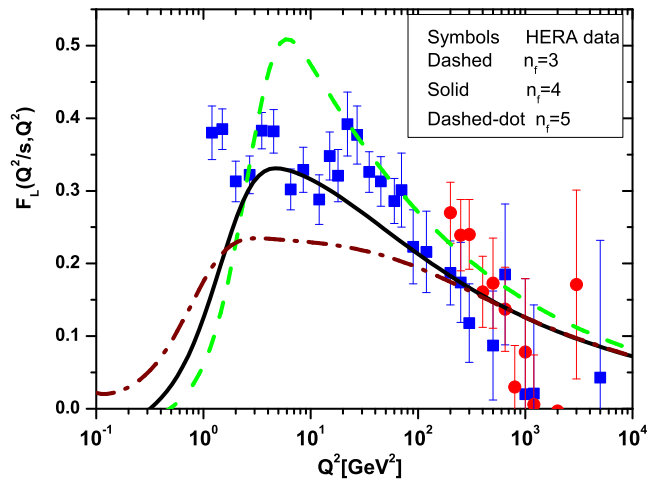


FIG. 4: The DIS longitudinal structure functions at the NLO approximation are shown by applying the active flavors ($n_f = 3$, green dashed curve), ($n_f = 4$, black solid curve) and ($n_f = 5$, brown dashed-dot curve) as a function of Q^2 for $\sqrt{s} = 318$ GeV based on the results in Table I and QCD cut-off. The HERA combined H1 and ZEUS reduced cross section datasets (squares-blue and circles-red) and their uncertainties are shown.

for light nuclei C-12 and heavy nuclei Pb-208 at x_{\min} in the kinematic range relevant for the EIC ($\sqrt{s} = 89$ GeV)², taking into account the rescaling variable due to the charm quark mass. We observe that the behavior of the nuclear

² The center-of-mass energies in electron-ion colliders proposed in China and the US are 15 – 20 GeV for EIC_C and 30 – 140 GeV for EIC respectively.

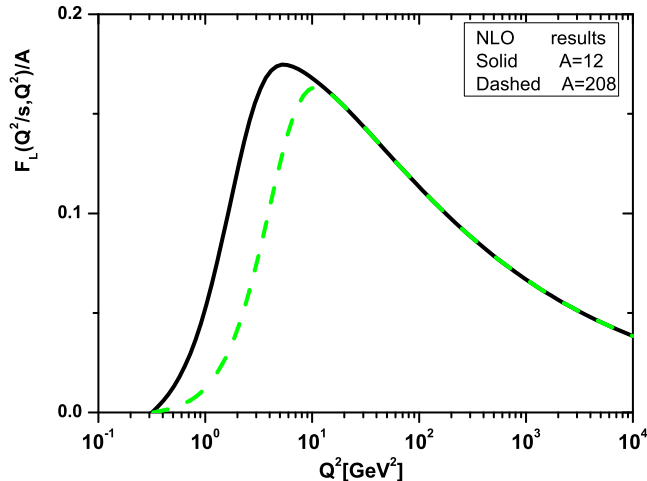


FIG. 5: The DIS longitudinal structure functions for light nuclei C-12 (black solid curve) and heavy nuclei Pb-208 (green dashed curve) at the NLO approximation are shown as a function of Q^2 for $\sqrt{s} = 89$ GeV. In these results the charm effect in the rescaling Bjorken variable x is considered. The coefficients are based on the results from Fit 1 in Table I.

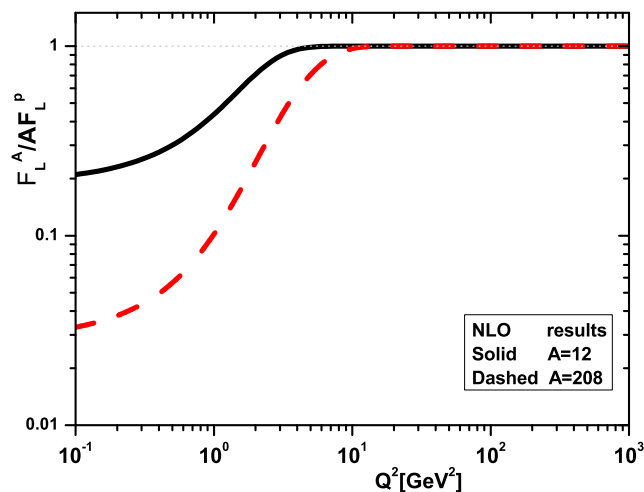


FIG. 6: Ratio of $\frac{F_L^A}{AF_L^P}$ for A=12 (black solid curve) and A=208 (red dashed curve) is shown as a function of Q^2 for $\sqrt{s} = 89$ GeV.

longitudinal structure function, $F_L^A(Q^2/s, Q^2)/A$, determines the transversely polarized photon-nuclei scattering at low Q^2 values. The enhancement of $F_L^A(Q^2/s, Q^2)/A$ decreases at moderate Q^2 values as the mass number A increases, and increases as Q^2 values increase. The behavior of $F_L^A(Q^2/s, Q^2)/A$ is independent of the mass number A at large Q^2 values.

Indeed, the parameter $k = A^{1/3}$ in Eq. (15) implements the enhancement of the saturation scale based on the gluon saturation, corresponding to an increase in the density of gluons [49]. This saturation is visible in large nuclei at low Q^2 values, as shown in Fig.5. The gluon saturation is tested by comparing the longitudinal structure functions in protons and nuclei. In Fig.6, the behavior of the ratio $\frac{F_L^A}{AF_L^P}$ is considered at the minimum value of

x given by Q^2/s at the EIC center-of-mass energy $\sqrt{s} = 89$ GeV. A clear deviation of the ratio $\frac{F_L^A}{AF_L^p}$ from the linearized description, which indicates the relevance of nonlinear terms, is visible in Fig.6 and is significant for large nuclei. The nonlinear effects begin for light and heavy nuclei at $Q^2 < 10$ GeV². The deviation of this ratio from unity demonstrates the significance of nonlinear effects, indicating saturation physics at x_{\min} . The results of saturation effects in eA collisions, conducted using the color dipole approach, confirmed the findings presented in Ref.[63]. The effect of different values of k ($k = 2.289$ and $k = 5.925$) on the behavior of the ratio at x_{\min} is visible in Fig.6 and may already be observable for photonuclear reactions, where gluon densities are enhanced by $A^{1/3}$.

In conclusion, we have examined the behavior of the longitudinal structure function of protons and nuclei at $y = 1$, where $x_{\text{Bj}} = x_{\min} = Q^2/s$, in both HERA and EIC kinematics. We utilized the expanding method and CDP for low x gluon distributions in this scenario. Our model provides a good description of results at moderate and large Q^2 values when compared to HERA data, and predicts nuclear longitudinal structure functions that can be measured in electron-ion collisions at x_{\min} . Comparing with HERA data at moderate and large Q^2 values strongly suggests that the gluon component is the dominant factor in the longitudinal structure function within the dipole picture. We observed that the value of F_L is small at low Q^2 values in the dipole picture. This is because the dominant gluon component is strongly suppressed and the polarization of the exchanged photon is transverse at this kinematic point. We investigated the nuclear longitudinal structure function at this limit, which reveals high gluon densities and associated nonlinear high-energy evolution. The nonlinear corrections increase with the mass number A . The ratio $\frac{F_L^A}{AF_L^p}$ can serve as an indicator for the presence of nonlinear low x dynamics in large nuclei.

APPENDIX A

The longitudinal structure function at the expanding points $z = 0$ and 0.666 is:

$$\begin{aligned} a = 0, \quad F_L(x, Q^2) &= \frac{2\alpha_s}{3\pi} F_2\left(\frac{4}{3}x, Q^2\right) + \frac{10\alpha_s}{27\pi} G\left(\frac{3}{2}x, Q^2\right) - \frac{28.440\alpha_s^2}{32\pi^2} F_2\left(\frac{3}{2}x, Q^2\right) - \frac{17.778\alpha_s^2}{32\pi^2} G\left(\frac{3}{2}x, Q^2\right), \\ a = 0.666, \quad F_L(x, Q^2) &= \frac{2\alpha_s}{3\pi} F_2(2x, Q^2) + \frac{10\alpha_s}{27\pi} G(2.5x, Q^2) - \frac{14.315\alpha_s^2}{16\pi^2} F_2\left(\frac{3}{2}x, Q^2\right) - \frac{8.948\alpha_s^2}{16\pi^2} G\left(\frac{3}{2}x, Q^2\right). \end{aligned} \quad (17)$$

APPENDIX B

The relationship between the gluon distribution and the dipole cross-section is defined by the dipole picture and the k_T -factorization theorem [60, 61]. The basic theoretical formula for F_L into the longitudinal photon polarization is

$$F_L(x, Q^2) = \frac{Q^2}{4\pi^2\alpha_{\text{em}}} \sigma_L^{\gamma^* p}(x, Q^2), \quad (18)$$

when the virtual photon dissociates into a quark-antiquark pair (a $q\bar{q}$ dipole), it subsequently interacts with the proton as

$$\sigma_L(x, Q^2) = \sum_f \int_0^1 dz \int d^2r |\Psi_L(r, z, Q)|^2 \hat{\sigma}(x, r^2), \quad (19)$$

where the sum over quark flavours f is performed as it depends on the contributions from the light quark pairs ($u\bar{u}$, $d\bar{d}$ and $s\bar{s}$) as well as the contributions from the $c\bar{c}$ and $b\bar{b}$ pairs. The photon wave function depends on the mass of the quarks in the $q\bar{q}$ dipole. Therefore the Bjorken variable x is modified to include the dipole cross section into the quark mass using the following form

$$x \rightarrow x \left(1 + \frac{4m_f^2}{Q^2}\right). \quad (20)$$

The dipole cross-section is

$$\hat{\sigma}(x, r^2) = \frac{4\pi^2}{3} \int \frac{dk^2}{k^4} \alpha_s f(x, k^2) (1 - J_0(kr)), \quad (21)$$

TABLE I: The coefficient values are obtained in Ref.[62].

fit	m_l [GeV]	m_c [GeV]	m_b [GeV]	σ_0 [mb]	λ	$x_0/10^{-4}$	χ^2/N_{dof}
0	0.14	-	-	23.58 ± 0.28	0.270 ± 0.003	2.24 ± 0.16	1.83
1	0.14	1.4	-	27.32 ± 0.35	0.248 ± 0.002	0.42 ± 0.04	1.60
2	0.14	1.4	4.6	27.43 ± 0.35	0.248 ± 0.002	0.40 ± 0.04	1.61

where $J_0(kr)$ is the Bessel function of the first kind and $f(x, k^2)$ is the unintegrated gluon distribution. The unintegrated gluon distribution is obtained in the following form [48]

$$f(x, k^2) = \frac{3\sigma_0}{4\pi^2\alpha_s} k^4 (x/x_0)^\lambda e^{-k^2(x/x_0)^\lambda}. \quad (22)$$

The integrated gluon distribution is obtained using the leading twist relation

$$xg(x, Q^2) = \int_0^{Q^2} \frac{dk^2}{k^2} f(x, k^2). \quad (23)$$

The three parameters (σ_0 , x_0 and λ) of the fits with the GBW model using the quark masses are listed in Table.I

ACKNOWLEDGMENTS

The author would like to thank F.E.Taylor and F.Salazar for their helpful comments and invaluable support. I am also very grateful to the Department of Physics at CERN-TH for their warm hospitality.

-
- [1] C.G.Callan, Jr. and D.J.Gross, Phys.Rev.Lett.**22**, 156 (1969).
[2] P. Agostini et al. (LHeC Collaboration and FCC-he Study Group), J. Phys. G **48**, 110501 (2021).
[3] EIC BNL, <https://www.bnl.gov/eic/>.
[4] V. Andreev et al. (H1 Collaboration), Eur. Phys. J. C **74**, 2814 (2014).
[5] H. Abramowicz et al. (ZEUS Collaboration), Phys. Rev. D **90**, 072002 (2014).
[6] A. Abada, et al., FCC Collaboration, Eur. Phys. J. C **79**, 474 (2019).
[7] M. Klein, arXiv:1802.04317[hep-ph]; Ann. Phys. **528**, 138 (2016).
[8] N. Armesto, et al., Phys. Rev. D **100**, 074022 (2019).
[9] E. Iancu, A. Leonidov, and L. McLerran, arXiv:hep-ph/0202270; E. Iancu and R. Venugopalan, arXiv:hep-ph/0303204; F. Gelis, E. Iancu, J. Jalilian-Marian, and R. Venugopalan, Ann. Rev. Nucl. Part. Sci. **60**, 463 (2010).
[10] A. Morreale and F. Salazar, Universe **7**, 312 (2021).
[11] B. Z. Kopeliovich, L. I. Lapidus, and A. B. Zamolodchikov, JETP Lett. **33**, 595 (1981).
[12] N. N. Nikolaev and B. Zakharov, Z.Phys. C **49**, 607 (1991).
[13] J.Bartels, K.Golec-Biernat, and H.Kowalski, Phys. Rev. D **66**, 014001 (2002).
[14] E.Iancu, K.Itakura, and S.Munier, Phys.Lett. B **590**, 199 (2004).
[15] J.Bartels and E.levin, Nucl.Phys. B **387**, 617 (1992).
[16] E.Iancu, K.Itakura, and L.McLerran, Nucl. Phys. A **708**, 327 (2002).
[17] P.Caucal and E.Iancu, Phys. Rev.D **111**, 074008 (2025).
[18] H.Mantysaari, J.Penttala, F.Salazar, and B.Schenke, Phys.Rev.D **111**, 054033 (2025).
[19] J. Jimenez-Lopez, P. R. Newman, and K. Wichmann, arXiv: 2412.16123 [hep-ph].
[20] Frank E.Taylor, Phys.Rev.D **111**, 052001 (2025).
[21] L. N. Hand, Phys. Rev. **129**, 1834 (1963).
[22] K.Gorlec-Biernat and M.Wusthoff, Phys. Rev. D **59**, 014017 (1998).
[23] P. Caucal and F. Salazar, arXiv[hep-ph]: 2502.02637.
[24] D.I.Kazakov et al., Phys.Rev.Lett. **65**, 1535 (1990).
[25] L.H.Orr and W.J.Stirling, Phys.Rev.Lett. **66**, 1673 (1991).
[26] L. P. Kaptari, A. V. Kotikov, N. Yu. Chernikova, and Pengming Zhang, Phys. Rev. D **99**, 096019 (2019).
[27] G. R. Boroun and B. Rezaei, Phys. Lett. B **816**, 136274 (2021).
[28] M.Niedziela and M.Praszalowicz, Acta Physics Polonica B **46**, 2018 (2015).
[29] N.Baruah, M.K.Das and J.K.Sarma, Eur.Phys.J. Plus **129**, 229 (2014).

- [30] G.R.Boroun, B.Rezaei and J.K.Sarma, *Int.J.Mod.Phys.A* **29**, 1450189 (2014).
- [31] K.Gorlec-Biernat and A.M.Stasto, *Phys. Rev. D* **80**, 014006 (2009).
- [32] A.D.Martin, W.J.Stirling and R.S.Thorne, *Phys. Lett. B* **635**, 305 (2006).
- [33] A.V.Kotikov and G.Parente, *Mod.Phys.Lett.A* **12**, 963 (1997).
- [34] M. Gluck, C.Pisano and E. Reya, *Phys.Rev.D* **77**, 074002 (2008).
- [35] S. Moch and A. Vogt, *JHEP* **0904**, 081 (2009).
- [36] M.Modarres, M.R.Masouminia, H.Hosseinkhani and N.Olanj, *Nucl.Phys.A* **949**, 168 (2016).
- [37] M.Mottaghizadeh and A.Mirjalili, *Phys.Lett.B* **820**, 136534 (2021).
- [38] S.Zarrin and S.Dadfar, *Int.J.Theor.Phys.* **60**, 3822 (2021).
- [39] G. Altarelli and G. Martinelli, *Phys. Lett. B* **76**, 89 (1978).
- [40] M. Gluck and E. Reya, *Nucl. Phys. B* **145**, 24 (1978).
- [41] S. Moch, J.A.M. Vermaseren and A. Vogt, *Phys. Lett. B* **606**, 123 (2005).
- [42] G.R.Boroun, *Phys. Rev.C* **97**, 015206 (2018).
- [43] G.R.Boroun and B.Rezaei, *Eur.Phys.J.C* **72**, 2221 (2012).
- [44] M. B. Gay Ducati and P. B. Goncalves, *Phys. Lett. B* **390**, 401 (1997).
- [45] J. X. Chen, X. P. Wang et al., *Chin. Phys. C* **48**, 063104 (2024).
- [46] G.R.Boroun and Y.Cai, *Chin. Phys. C* **49**, 053104 (2025).
- [47] G.R.Boroun, *Commun. Theor. Phys.* **77**, 055201 (2025).
- [48] R. S. Thorne, *Phys. Rev. D* **71**, 054024 (2005).
- [49] M.A.Peredo and M.Hentschinski, *Phys.Rev.D***109**, 014032 (2024).
- [50] F Carvalho, F O Duraes, F S Navarra and S Szpigiel, *Phys. Rev. C* **79**, 035211 (2009).
- [51] N. Armesto, H. Paukkunen, C. A. Salgado, and K. Tywoniuk, *Phys.Lett.B* **694**, 38 (2010).
- [52] N. Armesto et.al., *Phys. Rev. D* **105**, 114017 (2022).
- [53] B.Rezaei, *Nucl. Phys. A* **1053**, 122971 (2025).
- [54] K. Kovarik et. al., nCTEQ15, *Phys. Rev. D* **93**, 085037 (2016).
- [55] H. Khanpour and S. Atashbar Tehrani, *Phys. Rev. D* **93**, 014026 (2016).
- [56] N Armesto, C A Salgado and U A Wiedemann, *Phys. Rev. Lett.* **94**, 022002 (2005).
- [57] D A Fagundes and M V T Machado, *Phys. Rev. D* **107**, 014004 (2023).
- [58] N. N. Nikolaev, W. Schafer, B. G. Zakharov, and V. R. Zoller, *JETP Lett.* **84**, 537 (2006).
- [59] HERAhepdata, <https://www.hepdata.net/record/ins1377206>.
- [60] S. Catani, M. Ciafaloni and F. Hautmann, *Nucl. Phys. B* **366**, 135 (1991) 135.
- [61] J. C. Collins and R. K. Ellis, *Nucl. Phys. B* **360**, 3 (1991).
- [62] K. Golec-Biernat and S. Sapeta, *JHEP* **03**, 102 (2018).
- [63] E. R. Cazaroto, F. Carvalho, V. P. Goncalves and F. S. Navarra, *Phys. Lett. B***671**, 233 (2009).